Quantitative Trace Element Analysis of Individual Fly Ash Particles by Means of X-ray Microfluorescence

ARTICLE *in* ANALYTICAL CHEMISTRY · APRIL 2002

Impact Factor: 5.64 · DOI: 10.1021/ac010789b · Source: PubMed

Anal. Chem. **2002,** *74,* 1128−1135

Quantitative Trace Element Analysis of Individual Fly Ash Particles by Means of X-ray Microfluorescence

L. Vincze*,[†] A. Somogyi,[†] J. Osán,[‡] B. Vekemans,[†] S. Török,[‡] K. Janssens,[†] and F. Adams[†]

Department of Chemistry, University of Antwerp (UIA), Universiteitsplein 1, B-2610 Antwerpen, Belgium, and KFKI Atomic Energy Research Institute, P.O. Box 49, H-1525 Budapest, Hungary

A new quantification procedure was developed for the evaluation of X-ray microfluorescence (XRF) data sets obtained from individual particles, based on iterative Monte Carlo (MC) simulation. Combined with the high sensitivity of synchrotron radiation-induced XRF spectroscopy, the method was used to obtain quantitative information down to trace-level concentrations from micrometer-sized particulate matter. The detailed XRF simulation model was validated by comparison of calculated and experimental XRF spectra obtained for glass microsphere standards, resulting in uncertainties in the range of 3−10% for the calculated elemental sensitivities. The simulation model was applied for the quantitative analysis of X-ray tube and synchrotron radiation-induced scanning micro-XRF spectra of individual coal and wood fly ash particles originating from different Hungarian power plants. By measuring the same particles by both methods the major, minor, and trace element compositions of the particles were determined. The uncertainty of the MC based quantitative analysis scheme is estimated to be in the range of 5−30%.

Many environmental and geological applications require the quantitative characterization of particulate matter or materials having grainlike structure. There are two major approaches in the analysis of particulate matter: bulk and single-particle analysis. By using bulk methods, only the average composition of the particulate sample can be obtained. However, these samples are heterogeneous mixtures of different types of particles, so the average composition and average diameter do not describe well the dispersion of the particles in the sample. Also, the deposition of inhaled dust along the human respiratory tract is strongly dependent on the size and compositional distribution of the particles, since one particle having elevated concentrations of toxic elements can cause a DNA change in one pulmonary cell, as a precursor of lung cancer.[1] A majority of research studies associated with on-line particle analysis is based on mass spectrometry or atomic emission spectroscopy as the analytical method for particle composition measurements. Various combinations of these analytical methods can be employed, realizing various approaches to real-time analysis of particle size and composition. A review of mass spectroscopy techniques for single-particle analysis can be found in ref 2.

The size distribution and qualitative organic and inorganic composition can be efficiently studied using aerosol time-of flight mass spectrometry (ATOFMS), allowing the on-line measurement of thousands of individual particles in a short time.[3] After accurate efficiency calibration, the method can be used effectively for the analysis of particles in the respirable size range (0.1−2.5 μm).[4] For larger particles, laser decomposition is not complete; only a part of the particle surface is ionized.

The major elements in individual microparticles can be quantitatively determined using electron probe X-ray microanalysis (EPXMA).[5,6] However, on the basis of the major element composition, only natural and anthropogenic particles cannot be identified unambiguously (consider, for example, soil-derived and fly ash particles). Therefore, accurate knowledge of the minor and trace composition of individual particles is of high importance for source profiling studies, as they offer more distinctive features for the identification of different particle sources. In this respect, a complementary method suitable for single-particle analysis, providing trace-level sensitivity, is proton-induced X-ray emission (PIXE), which offers a valuable alternative to automated EPXMA.[7,8]

In this paper, we focus on X-ray microfluorescence (XRF) spectroscopy as an important analytical tool for determining the composition of microscopic samples down to trace concentration levels. The method is appreciated for its high sensitivity and nondestructiveness and because of its simple relation to the

[†] University of Antwerp.

[‡] KFKI Atomic Energy Research Institute.

(1) Balásházy, I.; Heistracher, T.; Hofmann, W. *J. Aerosol Med.* **1996**, *9*, 287−301.

(2) Noble, C. A.; Prather, K. A. *Mass Spectrom. Rev.* **2000**, *19* (4), 248−274.

(3) Prather, K. A.; Nordmeyer, T.; Salt, K. *Anal. Chem.* **1994**, *66*, 1403.

(4) Allen, J. O.; Fergenson, D. P.; Gard, E. E.; Hughes, L. S.; Morrical, B. D.; Kleeman, M. J.; Gross, D. S.; Gälli, M. E.; Prather, K. A.; Cass, G. R. *Environ. Sci. Technol.* **2000**, *34*, 211.

(5) Fruhstorfer, P.; Niessner, R. *Mikrochim. Acta* **1994**, *113*, 239−250.

(6) Osán, J.; Szalóki, I.; Ro, C.-U.; Van Grieken, R. *Mikrochim. Acta* **2000**, *132*, 349−355.

(7) Cereda, E.; Braga, G. M.; Pedretti, M., Grime G. W.; Baldacci, A. *Nucl. Instrum. Methods* **1995**, *B104*, 625−629.

(8) De Bock, L.; Van Grieken, R.; Camuffo, D.; Grime, G. *Environ. Sci. Technol.* **1996**, *30*, 3341.

10.1021/ac010789b CCC: $22.00
Published on Web 01/15/2002

fundamental physics of atom−radiation interaction.[9] This relation is normally expressed in terms of the so-called fundamental parameter models (FPM) used for quantifying the XRF results.[10] With the rise of the FPM in combination with the energy-dispersive solid-state detectors in the early 1960s, XRF developed into a multielemental method capable of providing analytical results from almost any kind of sample without any a priori analytical information or calibration procedure.

Generalized iterative procedures based on FPM for quantitative XRF analysis were published by many authors; see, e.g., refs 11 and 12. In general, the estimation of the matrix attenuation for the iterative calculation is based on the average atomic number of the sample matrix. The procedure offers a wide range extension for quantitative standardless XRF analysis of complex samples, especially for environmental and biological materials. In contrast to these methods, our approach uses the Monte Carlo (MC) technique, which is becoming a viable and more general alternative to FPM in view of the rapidly increasing availability of affordable computing power in recent years.

The majority of the laboratory-scale XRF instruments are applied as a bulk analytical technique. By introducing capillary optics,[13] the beam size can be reduced to microscopic range, typically down to 10−100 μm, allowing the examination of individual microparticles. Several papers appeared on the applicability of microscopic XRF for the analysis of particulate matter without aiming the determination of trace element concentrations quantitatively.[14,15] Lankosz and Pella applied the FPM for quantitative XRF analysis of individual particles having irregular shapes, but only for major and minor elements.[16] The theoretically derived calculations were verified by analysis of standard glass particles with known stoichiometry, and an agreement within 3−10% was found between calculated and nominal concentrations. The measurements were performed by the use of an X-ray microbeam with 177-μm diameter.

It has been shown that, with the use of micrometer-sized X-ray beams, topological variation can be distinguished from chemical inhomogeneities by looking at the correlation between the intensities from the different elements.[17] Thus, by using microbeam XRF in scanning mode, it is possible to separate the impact of chemical inhomogeneities and sample topology. For quantitative trace element analysis, the different matrix and attenuation effects caused by the differences in the size and shape of the particle have to be taken into account accurately. Also, the intensity variation over the X-ray microbeam has to be described well. Therefore, conventional quantification methods cannot be used for trace element analysis of individual microparticles.

Within the framework of a three-dimensional ray tracing-based MC method the XRF spectra can be simulated for arbitrary homogeneous or heterogeneous structures.[18−20] This approach yields good agreement between simulated and experimental data for individual standard microparticles. A considerable advantage of the Monte Carlo simulation model compared to analytical calculations based on FPM is its little restrictions on the complexity of the simulated sample and environment and the fact that it can be used reliably to simulate several consecutive interaction orders, such as multiple scattering or enhancement. In this way, the effects of sample environment (such as the scattering contribution by the surrounding air), sample topological effects to the detected line intensities, or interelement enhancement phenomena can easily be studied.

The aim of the present research is to develop a quantitative analytical method capable of determining minor and trace element concentrations in individual particles. The method is based on Monte Carlo simulations for dealing with the energy and spatial distribution of the X-ray microbeam, the interaction between the exciting photons and the sample elements taking into account the geometry effects caused by the size and topology of the particles. The applicability of the method is demonstrated on fly ash particles because they are common atmospheric particles having relatively elevated concentrations of some toxic elements.

In what follows, first the experimental apparatus is described for our micro-XRF experiments on fly ash particles, followed by the brief description of the XRF Monte Carlo simulation code used for quantification. Then the validation of the code is presented, based on comparison of simulated and experimental data on glass microsphere reference materials of known stoichiometry. Finally, the application of the MC based quantification method for individual wood and coal fly ash particles originating from different power plants is presented.

EXPERIMENTAL SECTION

Instruments. Two instruments were used: a laboratory-size micro-XRF setup and a synchrotron-based micro-XRF spectrometer. Figure 1a shows the schematic layout of the laboratory scale micro-XRF spectrometer of the University of Antwerp. A rotating-anode Mo X-ray tube was used for generating the primary beam coupled with a tapered glass monocapillary having 15-μm exit diameter. The latter produced an X-ray microbeam of about 20−25 μm on the sample using a working distance of 1 mm. A Canberra Si(Li) detector of 80 mm^2 active area having a resolution of 170 eV (fwhm) at Mn Kα (Mn K-L$_{2,3}$) was employed for detecting the fluorescent spectra. Typical live time was 2700 s, corresponding to a 3 × 3 two-dimensional scan of the particle of 300 s. The sum spectrum of such a scan corresponds to a full illumination of the particle, averaging the spatial inhomogeneities of its composition.

At Hasylab Beamline L (Figure 1b), the white X-ray beam produced by a 1.2-T bending magnet of the Doris-III storage ring was used for excitation. The energy of the excitation beam covers the 2−80-keV range. The low-energy part of the spectrum can be

(9) Jenkins, R.; Gould, R. W.; Gedcke, D. *Quantitative X-ray Spectrometry*; Marcel Dekker: New York, 1981.
(10) Van Espen, P.; Janssens, K.; Nobels, J. *Chemom. Intell. Lab. Syst.* **1986**, *1*, 109−114.
(11) Szalóki, I.; Lewis, D. G.; Benett, C. A.; Killic, A. *Phys. Med. Biol.* **1999**, *44*, 1245−1255.
(12) He, F.; Van Espen, P. *Anal. Chem.* **1991**, *63*, 2237−2244.
(13) Janssens, K.; Vekemans, B.; Vincze, L.; Adams, F.; Rindby, A. *Spectrochim. Acta* **1996**, *B51* (13), 1661−1678.
(14) Török, Sz.; Faigel, Gy.; Osán, J.; Török, B.; Jones, K. W.; Rivers, M. L.; Sutton, S. R.; Bajt, S. *Adv. X-Ray Anal.* **1994**, *37*, 711−716.
(15) Rindby, A.; Engström, P.; Janssens, K.; Osán, J. *Nucl. Instrum. Methods Phys. Res.* **1997**, *B124*, 591−604.
(16) Lankosz, M.; Pella, P. A. *X-Ray Spectrom.* **1997**, *26*, 347−349.
(17) Rindby, A.; Voglis, P.; Attaelmanan, A. *X-Ray Spectrom.* **1996**, *25*, 39−50.
(18) Vincze, L.; Janssens, K.; Adams, F.; Rivers, M. L.; Jones, K. W. *Spectrochim. Acta* **1995**, *B50*, 127−148.
(19) Vincze, L.; Janssens, K.; Adams F. *Spectrochim. Acta* **1993**, *B48*, 553−573.
(20) Vincze, L.; Janssens, K.; Vekemans, B.; Adams, F. *J. Anal. At. Spectrom.* **1999**, *14* (3), 529−533.

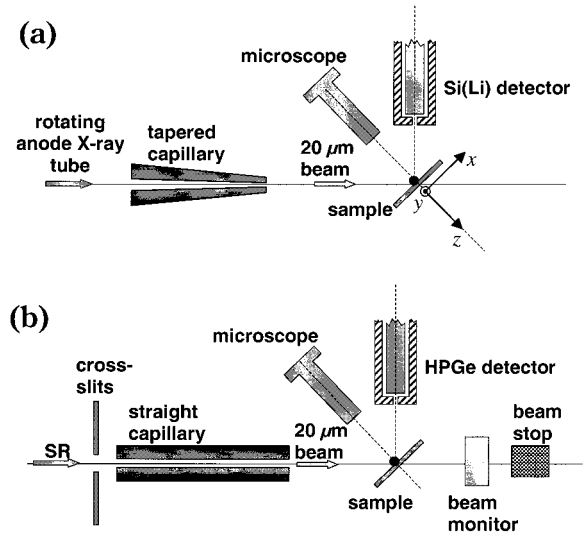

Figure 1. Top view of the rotating anode X-ray tube-based laboratory instrument (a) and the micro-SRXRF setup installed at Beamline L, Hasylab (b). In both cases, the microscope optical axis defines the *z* axis of the employed coordinate system, which also corresponds to the sample normal. During a horizontal scan, the sample is translated along the axis *x*, while a vertical scan is performed along the axis *y*.

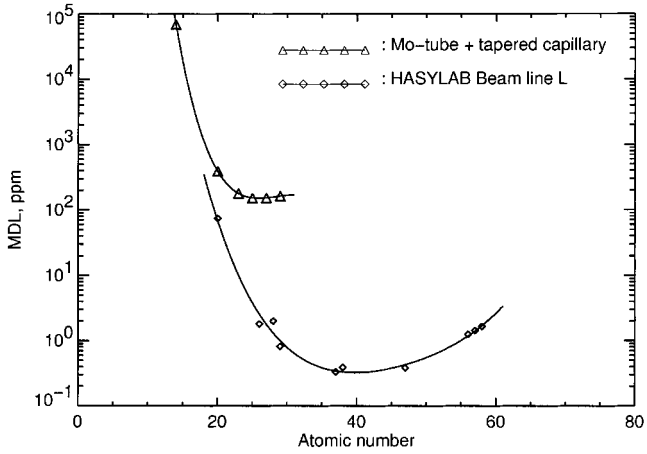

Figure 2. Relative detection limits obtained at Hasylab Beamline L and using the rotating anode X-ray tube-based laboratory XRF spectrometer at a live time of 300 s. The detection limit values were derived using a glass standard NIST SRM 612 (100-μm thickness) for the synchrotron setup and from a thin glass calibration standard NIST SRM 1832 for the laboratory instrument.

filtered by applying various beam absorbers. A motor-controlled cross-slit system was used for the collimation of the X-ray beam immediately before a parallel borehole borosilicate glass capillary of 20-μm inner diameter. An X-ray beam of ~20-μm diameter at the sample plane was produced using this straight capillary. The characteristic X-ray lines were detected with a high-purity germanium (HPGe) detector with an active crystal area of 30 mm^2 having a resolution of 170 eV (fwhm) at Mn Kα. Typical live times for spectrum recording were 300 s. In both setups, the sample was mounted onto an XYZ motor stage which, coupled with a positioning and data acquisition software, made the automatic measurement of a large number of particles possible.

The experimentally determined relative detection limits are shown in Figure 2. These results were obtained at Hasylab Beamline L using a NIST SRM 612 trace element glass standard having a thickness of 100 μm, corresponding to a live time of 300 s. As illustrated here, this SRXRF spectrometer provides (sub-)ppm-level detection limits for a wide range of elements. Also shown are the relative detection limits obtained for the laboratory spectrometer.

Samples. To validate the MC simulation and the quantification method, particulate standard samples were prepared from a microsphere glass standard reference material (NBS SRM K961). The diameter of the investigated particles was in the 20−60-μm range. The particles were suspended in *n*-hexane containing rubber cement (Talens' rubber cement, Royal Talen) and were then filtered through a Nuclepore membrane filter. Rubber cement was found to be an ideal fixing material, containing trace elements in very low concentration in a low-*Z* element matrix and providing elastic fixing.

Fly ash particles were collected at different Hungarian fossil power and heating plants. A coal-burning power plant (Tisza-palkonya) and a waste wood-burning heating plant (Pásztó) were chosen as sampling sites. Particles from the flue gas were collected isokinetically through a heated pipe to avoid condensation. The sample backing was a Nuclepore (0.8 mg/cm^2) polycarbonate filter. The volume of the pumped gas was 200 L. Fly ash samples were also collected from the flue gas particle collectors, such as from the electrostatic precipitator of the coal-burning plant and the bag filter of the wood-burning plant. These particles were further treated the same way as the standard particles. A total number of 100 individual particles were analyzed by micro-XRF.

THEORY

(1) XRF Simulation Model. The simulation model is based on the Monte Carlo technique; describing the relevant photon−matter interactions as a photon beam in the X-ray regime of 1−100 keV illuminates an arbitrary heterogeneous specimen. The exciting radiation can have any given (numerically defined) energy distribution in the above energy range and can be either unpolarized or linearly polarized. The modeled multielement sample can contain a maximum 92 elements from H to U. The simulated interaction types are as follows: the (i) photoelectric effect, followed by the emission of a fluorescence photon or Auger electron; (ii) Rayleigh (elastic) scattering; (iii) Compton (inelastic) scattering; (iv) photoelectron bremsstrahlung. Detailed description of the code can be found elsewhere.[18−20]

By simulating a statistically significant number of these interactions within the sample and its environment (e.g., surrounding air) and calculating the probability of subsequent fluorescence or scattered X-ray emission within the solid angle of the modeled detector, the complete spectral response of a given sample can be calculated.

The simulated spectrum can be compared directly to the experimental data in its entirety, including the scattered background of the XRF spectra, as well as the fluorescence line intensities. In the past, the model has been applied in an iterative manner for the quantitative XRF analysis of homogeneous bulk samples in much the same way as other quantification algorithms based on the fundamental parameter approach. Relative deviations in the range of 2−15% have been achieved by the Monte Carlo quantification scheme, depending on the analyzed element and

sample type.[18,19] Errors are mostly due to the uncertainties in the physical constants (cross sections, fluorescence yields, transition probabilities, etc.) applied in the simulations. The simulation-based algorithm used here is applied to particles with an assumed spherical geometry. This approximation was found to be reasonable from earlier EPXMA studies on the investigated particles. It can be shown that moderate deviations from the spherical shape do not influence significantly the accuracy of the analytical results for higher-*Z* trace elements, as their contribution and sensitivity to matrix absorption effects are in general small.

(2) Quantification Algorithm. In the case of a small, homogeneous particle that is irradiated fully by the primary beam, the detected characteristic X-ray line intensity $I_{i,\mathrm{meas}}$ of element i can be expressed as

$$I_{i,\mathrm{meas}} = I_0 C_i S_i \mathrm{Abs}_i \tag{1}$$

where I_0 is the intensity of the primary X-ray beam, C_i is the concentration of element i within the particle, S_i the elemental sensitivity value of element i, and Abs_i is a term describing the self-absorption of both incident beam and emitted characteristic X-ray line within the particle.

The $I_{i,\mathrm{meas}}$ net-peak intensity values can be determined by fitting the experimental spectra using a nonlinear least-squares fitting algorithm (AXIL).[21] The $I_0 S_i$ elemental yield values can be obtained experimentally by measuring thin standard reference samples under identical measuring conditions. The sensitivity values of elements for which standard samples are not available can be obtained by interpolating from the experimentally determined $S(Z_i)$ function. The element dependent self-absorption term Abs_i for a given particle depends on its topology and matrix composition.

In general, the irradiated mass, the shape, and the matrix of the particles are not known and it is very difficult to determine these parameters experimentally. That is why it is necessary to make some a priori assumptions on the basis of independent bulk measurements.

In our study, the shape of the particles was assumed to be spherical. The diameter of the particle-sphere was estimated using optical microscopy. An average density determined for the coal and wood fly ash by bulk pycnometry was used during the calculations. It was assumed that each element with a detectable X-ray line is present in its most common oxide form in the particle, such as SiO_2, SO_3, K_2O, CaO, TiO_2, and Fe_2O_3. All other elements were assumed to be present in atomic form. The sum of the elemental and oxide concentrations was assumed to be 100% in the case of coal fly ash. On the other hand, the sum was assumed to be 50% in the case of wood fly ash, the average organic content of which was ~50% according to thermal decomposition analysis. The remaining 50% of the matrix of the wood fly ash particles was assumed to consist of carbon.

The concentration values were calculated by an iterative Monte Carlo simulation method taking into account not only self-absorption within a spherical particle but also more subtle higher-order effects, such as interelement enhancement or fluorescence induced by in-sample scattering. To get the initial concentration values, necessary to start the iteration, self-absorption was neglected as a first step (i.e., $\mathrm{Abs}_i = 1$). The initial concentration of element i, $C_{i,0}$ with detectable X-ray line was calculated as

$$C_{i,0} = \frac{I_{i,\mathrm{meas}}/S_i}{\sum_{j=m+1}^{n} I_{j,\mathrm{meas}}/S_j}\left(1 - \sum_{j=1}^{m} C_j\right) \tag{2}$$

where n is the total number of elements in the sample and the first m elements constitute the dark matrix (which can be derived from stoichiometry or known from other, bulk measurements).

Using the assumption about the abundance of the elements in their most common oxide forms, the total amount of O can be calculated from simple stoichiometric considerations. Since the sum of the elemental concentrations and of the oxygen was assumed to be 100% for coal and 50% for wood fly ash, the first, initial concentration values can be determined.

As a second step, the above detailed Monte Carlo simulation code was used to iteratively refine these initial concentration values. As a density, an average value determined by bulk pycnometry was used (1.65 g/cm^3 for coal fly ash and 0.8 g/cm^3 for wood fly ash). On the basis of these assumptions, it is possible to calculate the self-absorption correction for the individual particles. The iterative procedure to refine the concentration of each element is given by

$$C_i^{(k+1)} = C_i^{(k)} \frac{I_{i,\mathrm{meas}}}{I_{i,\mathrm{calc}} \sum_{j=1}^{n} C_j^{(k)} \frac{I_{j,\mathrm{meas}}}{I_{j,\mathrm{calc}}}} \tag{3}$$

where $C_i^{(k)}$ is the calculated concentration of element i after k iteration steps.

The procedure is terminated, if either of the following conditions are met:

$$|C_i^{(k+1)} - C_i^{(k)}| < \epsilon \tag{4}$$

$$\sum_{i=1}^{n} \frac{(I_{i,\mathrm{meas}} - I_{i,\mathrm{calc}})^2}{\sigma_{i,\mathrm{meas}}^{\ 2}} < \delta \tag{5}$$

where $\sigma_{i,\mathrm{meas}} = I_{i,\mathrm{meas}}^{1/2}$ is the statistical uncertainty of the measured intensity corresponding to element i and the constants are chosen to be $\epsilon = 10^{-6}$ and $\delta = 10^{-2}$ to provide convergence in less than 10 iteration steps.

The trace element content of the particles was derived from the μ-SRXRF measurements by using the matrix composition determined for each individual particle separately using the laboratory system.

RESULTS AND DISCUSSION

(1) Validation of the MC Code Using Glass Microspheres. To evaluate the simulation code for calculating the spectral response of irradiated spherical particles, simulated X-ray fluorescence (point) spectra and line scans of NBS glass microsphere

(21) Vekemans, B.; Janssens, K.; Vincze, L.; Adams, F.; Van Espen, P. *X-Ray Spectrom.* **1994**, *23*, 278.

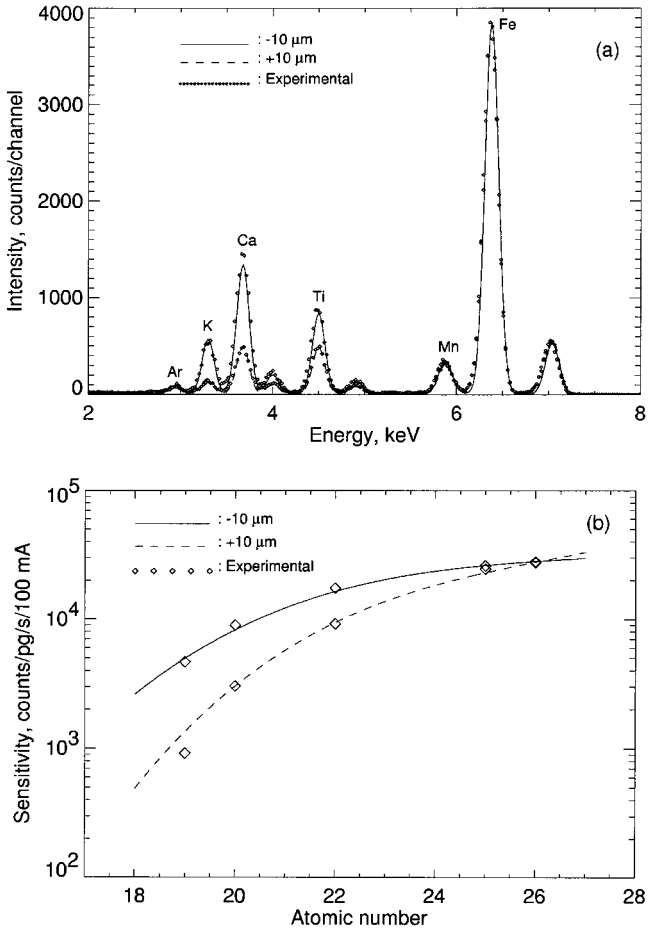

Figure 3. (a) Experimental and simulated XRF spectra measured at two different locations (±10-μm horizontal shift from the particle center) of a glass microsphere particle (NBS SRM K961) of 32-μm diameter. (b) Operational elemental sensitivities (elemental yields) corresponding to the above spectra.

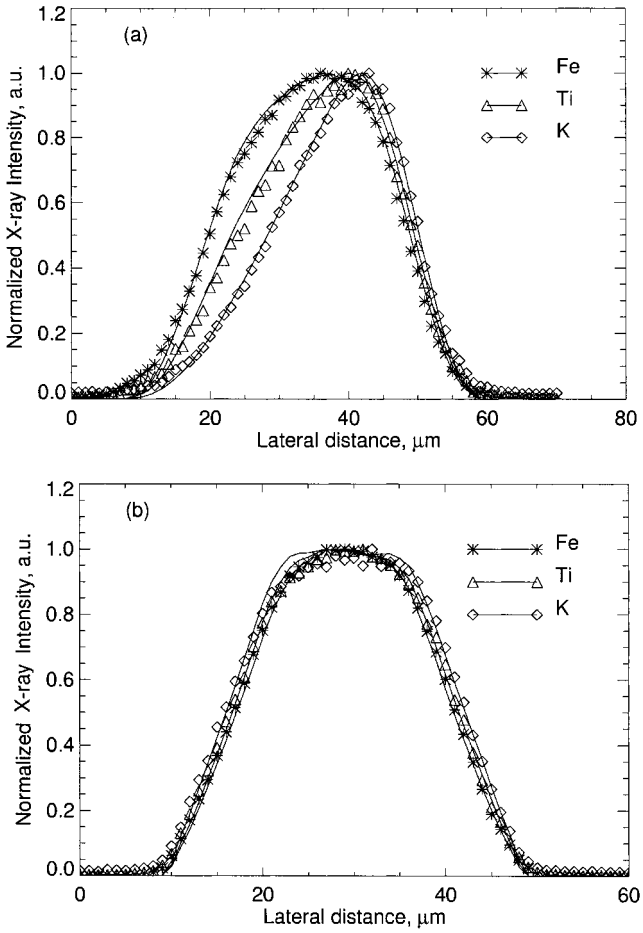

Figure 4. Elemental intensity distributions obtained from (a) horizontal and (b) vertical line scans through the center of the glass microsphere particle whose spectra are shown in Figure 3a. Symbols represent experimental values; lines indicate simulated scans.

standards were compared to experimentally recorded data. The experimental arrangement in these validation studies was identical to that illustrated in Figure 1b with the exception of using a pinhole instead of capillary optics to generate an 8-μm polychromatic SR beam at the National Synchrotron Light Source (NSLS; Brookhaven, NY) X26A beam line.

An example of the comparison of simulated and experimental XRF spectra of an NBS K961 glass microsphere, having a diameter of 32 μm, is shown in Figure 3a. The spectra correspond to two different horizontal particle positions along the x axis (see Figure 1a): +10 and −10 μm of the microbeam with respect to the particle center. The agreement between simulation and experiment is very good for both beam positions, indicating that the simulation takes into account correctly the variation of characteristic line intensities with (relative) beam position changes. While the primary excited volumes in both positions are identical, the escape paths of the induced fluorescent X-rays propagating toward the detector differ considerably, causing a significant difference between the recorded fluorescent spectra at their low-energy regions (E < 5 keV). By positioning the microbeam at these two locations of the particle, for example, the Ca/Fe intensity ratio changes by a factor of 3 due to their different absorption in the glass matrix.

It is evident that the elemental yields (defined as the net elemental count rates per irradiated elemental mass) are also dependent on the exact position of beam impact. This is shown in Figure 3b, where the simulated and experimental elemental yield curves are compared for the two beam positions, normalized to the Fe Kα peak. Here, the symbols represent experimental data, while the curves correspond to fitted polynomials to simulated elemental yields. In both cases, the calculated deviations between simulation and experiment are comparable to the statistical uncertainties of the recorded line intensities.

Figure 4 shows the variation of K, Ti, and Fe Kα net intensities corresponding to (a) a horizontal (direction x) and (b) a vertical (direction y) line scan through the particle center. The displayed simulated and experimental data show good agreement. In the case of the horizontal scan (see Figure 4a), at various beam positions on the particle the detected fluorescent intensity will change since the excited volume and the attenuation are different. Due to energy-dependent matrix absorption effects, these curves have different shapes for different atomic numbers. These matrix absorption effects in the glass sphere can be clearly seen in Figure 4a. While the recorded intensity distribution is almost symmetric for Fe Kα for which the glass of this thickness is fairly transparent, for K Kα, the maximum of the distribution is shifted significantly toward the edge closer to the detector. In the case of the vertical

Table 1. Calculated Elemental Concentration Values for a Glass Microsphere of 32 μm in Diameter,[a] Derived for Different Beam Positions (−5 and 5 μm) Relative to the Particle Center

	beam position				
	center	−5 μm		+5 μm	
element	true concn (%)	calcd (%)	rel dev (%)	calcd (%)	rel dev (%)
K	2.49	3.36	+35	1.49	−40
Ca	3.57	4.51	+26	2.27	−35
Ti	1.2	1.38	+15	0.88	−26
Mn	0.32	0.34	+6	0.27	−16
Fe	3.5	3.58	+2	3.0	−14
Ni	100 ppm	100.7 ppm	+0.7	87.3 ppm	−13
Zn	100 ppm	98.6 ppm	−1.4	89.1 ppm	−11
Br	100 ppm	97.0 ppm	−3	94.1 ppm	−6
Zr	100 ppm	96.3 ppm	−4	94.4 ppm	−6

[a] Major composition is assumed to be identical with that of NBS K961, doped with 100 ppm trace levels of Ni, Zn, Br, and Zr,

(direction *y*) scan (see Figure 4b), the recorded intensity distributions are symmetric as expected, exhibiting only a broadening of the plateau with decreasing X-ray energy. The good agreement between simulated and experimental scans demonstrates the ability of the simulation model to take into account correctly self-absorption effects for the specific case of spherical particles.

Furthermore, the examples above illustrate that the quantitative analysis of individual particles must be done with special care as, mainly due to sample self-absorption, the measured line intensity (and elemental sensitivity) ratios are strongly dependent on topological effects even for a homogeneous particle.

To demonstrate this more quantitatively, the effects of an uncertainty of 5 μm in the exciting beam position relative to the center of a 32-μm glass particle were estimated by the MC code, while in the quantification step the beam was assumed to illuminate the particle center. The results are summarized in Table 1, indicating that a relative error of up to 40% in the calculated concentrations may be the result of such an uncertainty in the actual beam position. The concentrations of low-*Z* elements, which are influenced most by absorption effects, are overestimated when the beam is on the detector side, while considerably underestimated when illuminating the particle away from the detector. In the case of homogeneous particles, irradiating the edge region of the particle on the detector side causes the reduction of self-absorption effects, which improves the sensitivity for low-*Z* elements. For accurate quantification in this particle size range, clearly a correct assumption has to be made with respect to the beam position relative to the particle center.

(2) Quantitative Analysis of Fly Ash Particles. As the simulation code reliably predicts the measured XRF intensities (and sensitivities) for the particulate standards, the model was applied for the quantitative analysis of unknown fly ash particles based on the iterative adaptation of the simulated concentrations (see eq 3).

The elemental compositions of 100 individual particles were calculated. In panels a and b of Figure 5, respectively, the measured and simulated XRF spectra of a typical coal and wood fly ash particle measured by the laboratory μ-XRF setup are shown. The agreement between the measured and simulated spectra is

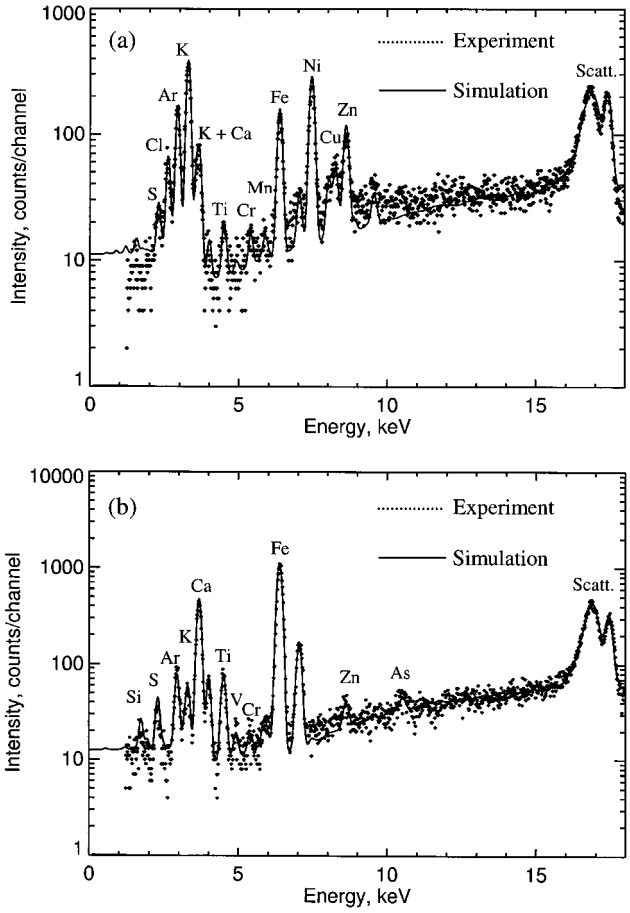

Figure 5. Measured (dots) and simulated (continuous line) XRF spectra obtained by the X-ray tube-based setup for a typical wood (a) and coal (b) fly ash particle.

satisfactory for both types of fly ash particles, both with respect to the fluorescence line and scatter peak intensities.

In Table 2, the initial and calculated major and minor element contents of the two particles are shown. In the case of the coal fly ash particles, the matrix is denser and the concentrations were calculated for two different densities (1.0 and 2.6 g/cm^3) in order to investigate the effect of its variation on the calculated concentrations. This is necessary since the density of individual particles may deviate significantly relative to the average bulk density of 1.65 g/cm^3. The chosen density range covers the density of glass (SiO_2), which is one of the main constituents of the fly ash matrix. It is clear from Table 2 that the self-absorption correction may change significantly with density. In the case of the coal fly ash particle, which serves as an example, the calculated concentration ratios for the two density values differ considerably (e.g., Fe/Si is 4.8/26 for $\rho = 2.6$ g/cm^3 and 7.6/23 for $\rho = 1.0$ g/cm^3).

The trace element content of the fly ash particles was determined from the μ-SRXRF measurements. Due to the long air path between the sample and detector (~4 cm), the characteristic peaks of the elements with atomic numbers lower than 19 (K) are only weakly present in the SRXRF spectra. Using the elemental composition of the (low-*Z*) fly ash matrix, determined from the tube-excited measurements and the above detailed assumptions, the trace element content of each individual fly ash particle could be determined in a single simulation step without the need for iteration. This is possible since elements with trace

Table 2. Major and Minor Element Concentrations of a Typical Fly Ash Particle

(a) Wood Fly Ash[a]

element	concentration (%) initial	calculated
O[b]	15	10
Si		
S	7	5
Cl	9	7
K	14	20
Ca	1.2	2.1
Ti	0.2	0.3
Cr	0.05	0.1
Mn	0.03	0.05
Fe	0.8	1.3
Ni	1.3	1.8
Cu	0.1	0.2
Zn	0.4	0.5

(b) Coal Fly Ash[c]

element	concentration (%) initial	calculated $\rho = 2.6$ g/cm^3	calculated $\rho = 1.0$ g/cm^3
O[b]	48	47	44
Si	27	26	23
S	7.0	8.3	7.4
K	1.5	1.7	1.9
Ca	9.8	12.0	13.9
Ti	0.7	0.9	1.1
Cr	0.05	0.05	0.07
Mn	0.08	0.07	0.10
Fe	6.3	4.8	7.6
Zn	0.07	0.05	0.08

[a] Corresponding experimental and simulated spectra shown in Figure 5a. The initial concentrations were calculated by neglecting the self-absorption within the particle; the calculated concentrations were obtained by assuming $\rho = 0.5$ g/cm^3 density and 50% carbon residual matrix. [b]Concentration value of oxygen was calculated from stoichiometric considerations. [c] Corresponding experimental and simulated XRF spectra shown in Figure 5b. The initial concentrations were calculated by neglecting the self-absorption within the particle; the calculated concentrations were obtained by assuming $\rho = 2.6$ g/cm^3 and $\rho = 1.0$ g/cm^3 density values of the particles, respectively.

concentration levels do not change the matrix absorption characteristics appreciably. In Table 3, the trace element composition of two particles are shown while in Figure 6 the corresponding experimental spectra measured at Hasylab Beamline L can be seen. It is clear from the table and from the spectra that the minimum detectable amounts of the investigated elements are much lower than in the case of the laboratory-scale microprobe setup although a much smaller measuring time (400 s) was chosen. In the case of the synchrotron setup, the quantitative determination of 10−100 ppm concentration levels is possible for elements with atomic numbers above 19 for fly ash particles of the investigated size range.

In Table 4. the average minor and major elemental concentrations and the variation in the particles of the wood and coal fly ash particles determined on the basis of 40 wood and 60 coal fly ash particles are shown. The same major elements could be detected in both types of fly ash, and these elements are visible in most of the particles. The major element concentration ratios are different in the two cases: in the case of wood fly ash, a higher concentration of S and Cl can be detected (originating from the organic component of the wood), while in case of the coal fly ash,

Table 3. Trace Element Concentrations in an Individual Wood and a Coal Fly Ash Particle (Spectra Shown in Figure 6a and b, Respectively)[a]

element	concentration (ppm) wood fly ash	coal fly ash
Se	21	53
Br	238	<5
Rb	148	170
Sr	100	415
Y	10	14
Zr	22	85
Nb	5	9
Mo	21	21
Ag	28	<5
Cd	117	<5
Sn	161	10
Sb	40	<5
Ba	588	440
Pb	1044	210

[a]In the case of the wood fly ash, a residual matrix consisting of 50% C and a density of 0.5 g/cm^3 was assumed, while in case of the coal fly ash, a density of 1.0 g/cm^3 was used.

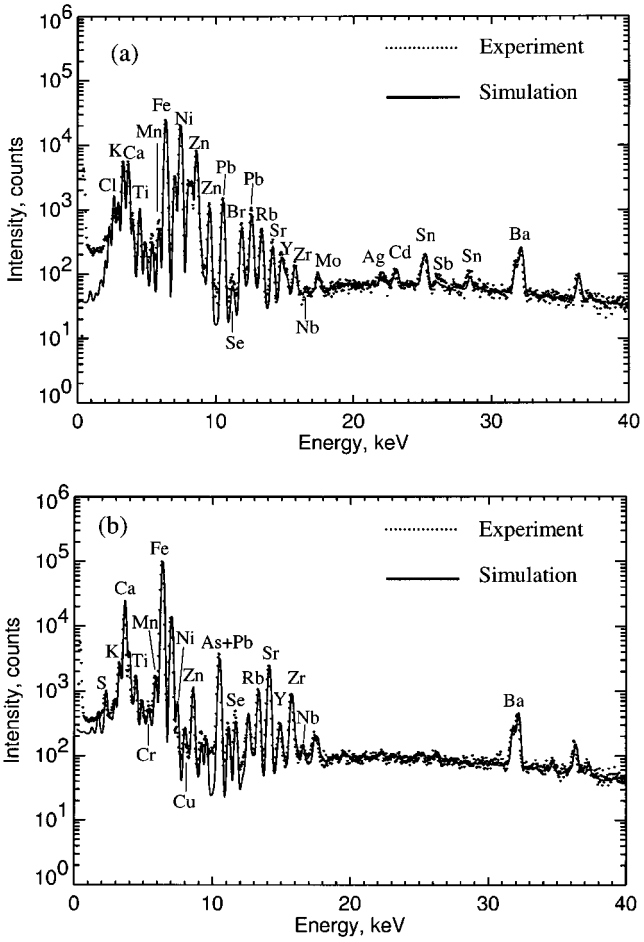

Figure 6. Experimental (dots) and simulated (continuous line) SRXRF spectra of the individual wood (a) and coal (b) fly ash particles shown in Figure 5.

the amount of elements characteristic to the minerals such as Si, Ca, and Fe is larger. In the case of coal fly ash, a higher number of potentially hazardous trace elements, e.g., Cu, As, and Pb, are detected. The variation of the elemental concentrations is large

Table 4. Average Major and Minor Element Concentrations of the Wood (50% C, $\rho = 0.5$ g/cm^3) and Coal Fly Ash ($\rho = 1.0$ g/cm^3) Particles Based on XRF Analysis by the X-ray Tube-Based Instrument[a]

	concentration (%)	
element	wood fly ash	coal fly ash
O[b]	12.6 ± 2.5	46 ± 4
Si	4.2 ± 2.1	25 ± 6
S	3.9 ± 1.3	8 ± 3
Cl	4.9 ± 2.3	0.4 ± 0.5
K	15.2 ± 4.3	1.9 ± 0.5
Ca	3.0 ± 2.7	12 ± 8
Ti	0.33 ± 0.13	0.3 ± 0.2
V	0.020 ± 0.024	
Cr	0.050 ± 0.026	0.03 ± 0.02
Mn	0.0605 ± 0.035	0.1 ± 0.1
Fe	2.7 ± 2.9	6 ± 4
Cu		0.03 ± 0.03
Zn	0.5 ± 0.2	0.069 ± 0.033
As		0.02 ± 0.02
Rb		0.02 ± 0.01
Sr		0.07 ± 0.07
Pb		0.017 ± 0.004

[a] Results were obtained on the basis of 60 individual coal and 40 wood fly ash particles. elements that were detected in less than 10 particles were not included into the table. [b]Concentration value of oxygen was calculated from stoichiometric considerations.

for both types of particles, showing the highly inhomogeneous nature of the ash material.

CONCLUSIONS

Quantitative trace element analysis of individual fly ash particles in the 20−60-μm size range is demonstrated by means of X-ray microfluorescence. Both X-ray tube and synchrotron radiation excited micro-XRF are well-suited methods for the sensitive elemental analysis of individual fly ash particles if the size of the particles is comparable or larger than that of the exciting beam. The synchrotron-based technique provides trace-level detection limits down to 10−100 ppm concentration levels.

The quantitative evaluation of the micro-XRF data sets is based on iterative Monte Carlo simulations by using a set of a priori assumptions for the shape, relying on optical microscopy for estimating the diameter, and separate bulk measurements, for determining the average density and organic material content, of the individual fly ash particles. The uncertainty level of the concentration values obtained by this combined method is estimated to be in the range of 5−30%.

It is shown that the sensitivity of XRF analysis for lighter elements can be improved by positioning the exciting X-ray microbeam to the edge region of the particle closest to the detector instead of its center corresponding to the maximum excitation volume. When the sensitivity for low-Z elements is optimized in this way, the uncertainty of the beam position can result in a significant overestimation of the calculated concentration levels for elements having the lowest detectable atomic numbers.

ACKNOWLEDGMENT

This work has been partially supported by the TMR Contract ERBFMGECT950059 of the European Union. L.V. is the fellow of the Belgian National Foundation for Scientific Research (FWO).

Received for review July 13, 2001. Accepted November 7, 2001.

AC010789B